



## 1 Air–Sea Interactions and Biogeochemical Responses to Medicane Daniel

2

3 Babita Jangir and Ehud Strobach

4 Institute of Soil, Water and Environmental Sciences, Volcani Institute, Agriculture Research  
5 Organization, Rishon LeTsiyon, Israel

6 \*Corresponding author: Babita Jangir (bj11@iitbbs.ac.in)

7

8 **Abstract:** Medicane Daniel, formed on 4-12 September 2023, has stood out as the deadliest  
9 recorded storm in Mediterranean history. In this study, we investigate the role of sea features  
10 as contributors to the intensification of the Medicane Daniel. Our findings reveal the presence  
11 of a warm core eddy (WCE), high ocean heat content, and a moderate marine heat wave  
12 (MHW) at the location where Medicane Daniel intensified. These features were situated near  
13 the coastal region, facilitating the Medicane's intensification close to the coast. Consequently,  
14 the Medicane did not weaken significantly after landfall, leading to severe damage along the  
15 coast of Libya. These conditions favoured the Medicane's intensification and, due to high  
16 moisture convergence, contributed to significant precipitation at the eddy and MHW position.  
17 Importantly, observations from the high-resolution Surface Water and Ocean Topography  
18 (SWOT) satellite captured the WCE more accurately or in finer detail. This allowed for  
19 attribution of changes in biogeochemical properties -namely, chlorophyll, phytoplankton,  
20 nutrients, and dissolved oxygen concentrations due to eddy-induced vertical mixing and  
21 upwelling. The biogeochemical properties tend to increase over the WCE and MHW locations  
22 due to mixing and upwelling induced by the presence of the WCE and MHW. Our case-study  
23 analysis suggests that, under atmospheric cyclone conditions, subsurface mixing may be more  
24 influential within CCEs than upwelling driven by Ekman pumping, which, by contrast, may  
25 play a more prominent role within WCEs.

26

27 **Key Words:** Medicanes, eddies, Marine Heat Wave, deadliest Medicane, SWOT satellite,  
28 Biogeochemistry

29

## 30 Key Points:

31

31     ● Along the path of Medicane Daniel, Warm Core Eddy (WCE), Ocean Heat Content,  
32         and Marine Heatwave (MHW) were present near the coastal region. Their combined  
33         presence enhanced precipitation, making Medicane Daniel a deadly storm.



34     ● SWOT satellite products better represent air-sea interaction due to their fine resolution  
35     over eddy regions.

36     ● An increase in surface chlorophyll was observed after the cyclone passed over the WCE  
37     location. Positive Ekman pumping confirms that the increase was caused by cyclone-  
38     induced upwelling.

39     ● Analysis of vertical profiles shows a decrease in surface temperature and an increase in  
40     chlorophyll and nutrient concentration above the mixed layer due to cyclone-induced  
41     mixing and upwelling.

42     ● Cross-section analysis over the WCE location shows an upward shift in isotherms,  
43     leading to increased chlorophyll from cyclone-induced mixing and upwelling.

44     **1. Introduction:**

45     The Mediterranean region (MR) is recognized as a climate change hotspot (IPCC, 2021),  
46     warming at a rate up to 1.5 times faster than the global average (MedECC, 2020; Zittis et al.,  
47     2022; Khodayar et al., 2025). Positioned between the arid climate of North Africa and the  
48     temperate and wet climate of Central Europe, the MR is particularly vulnerable to future  
49     climate impacts. Surface temperature in this region is projected to continue increasing, but the  
50     precipitation tends to decrease (Cherif et al., 2020; Reale et al., 2022). As a consequence, the  
51     magnitude of extreme phenomena such as Mediterranean cyclones, marine heat waves (MHW),  
52     and intense droughts is projected to increase under future climate scenarios (MedECC, 2020;  
53     Hochman et al., 2021; Zittis et al., 2022).

54  
55     Medicanes are a subcategory of Mediterranean cyclones, which can resemble hurricanes in  
56     both intensity and impact. They often bring torrential rainfall, flash floods, powerful winds,  
57     storm surges, and hazardous sea conditions. Such events pose significant risks, particularly to  
58     coastal communities and urban centers, threatening homes, livelihoods, and natural ecosystems  
59     (Hochman et al., 2021; Khodayar et al., 2025). Similar to Mediterranean cyclones, their  
60     intensity is projected to increase under future climate scenarios, but with lower frequency  
61     (González-Alemán et al., 2019). Despite their strong impact, the full extent of the damage  
62     medicanes inflict, both socially and economically, remains insufficiently understood.  
63     Moreover, their potential impact on ocean biogeochemistry is under-researched and often  
64     inadequately communicated, leaving a critical gap in public awareness and scientific insight.

65



66 Medicanes are also known as ‘tropical-like cyclones’ because they have cyclone-like  
67 characteristics such as a cloud-free calm “eye,” spiraling cloud bands, and strong winds near  
68 the vortex center. These features may be associated with the absence of fronts, weak vertical  
69 wind shear, and a warm core (WC) with an axisymmetric structure (Miglietta et al., 2019;  
70 Flaounas et al., 2022; Panegrossi et al., 2023). The formation of cyclones in the MR, including  
71 medicanes, is primarily driven by baroclinic instability and Rossby wave breaking (Raveh-  
72 Rubin and Flaounas, 2017; Flaounas et al., 2022). As these systems evolve and reach their  
73 mature stage, medicanes can intensify and be sustained through exchanges of heat and  
74 momentum at the air-sea interface (Emanuel, 2005). The development of intense  
75 Mediterranean cyclones is frequently associated with southward shifts of the polar jet, which  
76 enable air masses with high potential vorticity (PV) to enter the MR, thereby initiating  
77 baroclinic instability similar to that observed during extratropical cyclone development over  
78 open oceans (Flocas, 2000; Trigo et al., 2002; Nicolaides et al., 2006; Fita et al., 2007; Claud  
79 et al., 2010; Kouroutzoglou et al., 2011; Flaounas et al., 2015). Raveh-Rubin and Flaounas  
80 (2017) identified Rossby Wave Breaking (RWB) as a frequent precursor to Mediterranean  
81 cyclogenesis, while Flaounas et al. (2015) further emphasized that the cyclogenesis  
82 environment in the region is characterized by strong horizontal shear, driving these cyclones  
83 to follow a typical baroclinic life cycle. Furthermore, Flaounas et al. (2025) also highlight the  
84 importance of these atmospheric variables in the genesis and intensification of Medicane  
85 Daniel. However, in this manuscript, we primarily focus on the Atmospheric and oceanic  
86 precursor that are most directly associated with Daniel’s intensification and associated  
87 precipitation.

88

89 Furthermore, the role of underlying ocean eddies and MHW in modulating the deepening of a  
90 cyclone is often overlooked. Recent studies have highlighted the critical role of ocean eddies  
91 and MHWs in modulating cyclone’s deepening in the MR (Jangir et al., 2023, 2024; Mishra et  
92 al., 2024; Strobach et al., 2024). In particular, Jangir et al. (2024) demonstrated the significant  
93 intensification of medicane Ianos due to the presence of a strong MHW, making it the only  
94 category 2 cyclone observed in the Mediterranean Sea (MS). In contrast, other medicanes such  
95 as Zorbas and Apollo intensified primarily due to the interaction with Warm Core Eddies  
96 (WCEs) along their paths. Mishra et al. (2024) reported that if we remove these SST anomalies  
97 from the path of medicane Ianos, the medicane will still form, but with a reduced intensity.  
98 Strobach et al. (2024) reported that ocean mesoscale eddies in the Eastern Mediterranean can  
99 significantly influence extreme weather, as shown during the heavy rainfall event in Israel that



100 occurred from January 8 to 10, 2020. High-resolution coupled ocean-atmosphere simulations  
101 captured the event more accurately than uncoupled ones. The study by Strobach et al. (2024)  
102 highlights how eddies can enhance atmospheric moisture and meso-cyclone development,  
103 intensifying local extremes.

104

105 As efforts continue to enhance the accuracy of cyclone intensity forecasts, the potential  
106 influence of eddies MHW, and OHC remains a critical yet less explored aspect, particularly  
107 within the Mediterranean context. To improve the prediction of Mediterranean cyclones and  
108 mitigate associated risks, a deeper understanding of air-sea interaction processes and the role  
109 of pre-existing oceanic conditions in cyclone genesis and intensification is essential. Recent  
110 studies have increasingly focused on these dynamics, exploring how air-sea exchanges affect  
111 not only medicanes intensity but also the ocean's biogeochemical responses (Jangir et al., 2023;  
112 Menna et al., 2023; Scardino et al., 2024; Avolio et al., 2024). Notably, Jangir et al. (2023)  
113 highlighted the influence of WCEs on the intensification of medicanes, demonstrating that eddy  
114 size also plays a critical role; larger eddies tend to promote stronger cyclones and heavier  
115 rainfall. In this particular study, we show the influence of eddies and MHW on the intensity of  
116 medicane Daniel.

117

118 Most of the studies use the satellite SLA altimetry data from the Copernicus Marine Services  
119 (CMEMS) for the detection of eddies. Here, we also use the Surface Water and Ocean  
120 Topography (SWOT) satellite data, which are available at high spatial resolution. The SWOT  
121 satellite provides the first-ever global observations of ocean dynamics at sub-mesoscale spatial  
122 resolutions (1–100 km). While traditional satellite products, such as those from the Copernicus  
123 mission, offer spatial resolutions of approximately 25 km globally and 12.5 km in the MS,  
124 SWOT's advanced wide-swath altimetry overcomes these limitations by achieving resolutions  
125 as fine as 250 m to 2 km. This enhanced capability enables the detection of small-scale ocean  
126 features that were previously unresolved. SWOT observations confirm the widespread  
127 presence of sub-mesoscale eddies and internal waves, particularly energetic in regions like  
128 western boundary currents and the Antarctic Circumpolar Current (Archer et al., 2025;  
129 Tranchant et al., 2025). This high-resolution data is especially valuable for studying ocean-  
130 atmosphere interactions, such as the role of eddies in cyclone intensification. In particular,  
131 SWOT's ability to capture the structure, intensity, and evolution of eddies provides critical  
132 insight into how these features influence heat transport, vertical mixing, and the modulation of  
133 cyclone intensity due to eddies. Thus, SWOT marks a transformative step in advancing our



134 understanding of fine-scale ocean processes and their implications for weather, climate, and  
135 marine biogeochemistry.

136

137 Cyclones are known to trigger substantial phytoplankton blooms ([Shang et al., 2015](#);  
138 [Chowdhury et al., 2020](#); [Liu et al., 2020](#)). These blooms are primarily attributed to cyclone-  
139 induced upwelling and vertical mixing, which transport cold, nutrient-rich, or chlorophyll-  
140 loaded water into the euphotic zone, stimulating phytoplankton bloom. Such storm-driven  
141 biological responses offer valuable insight into ocean mixing and biogeochemical dynamics  
142 ([Chen et al., 2022](#)). Additionally, strong cyclonic winds often cause a noticeable decrease in  
143 SST, which plays a crucial role in regulating primary productivity ([Latha et al., 2015](#)). There  
144 are few studies reported in the other ocean basins that indicate the enhancement of chlorophyll-  
145 a (Chl-a) concentration following the passage of a cyclone in the presence of eddies ([Dutta et](#)  
146 [al., 2019](#); [Zhang and Qui, 2020](#); [Vidya et al., 2021](#)) and MHW ([Oliver et al., 2018](#); [Jangir et](#)  
147 [al., 2024](#)). Recently, a study by Scardino et al. ([2025](#)) reported the response of Mediterranean  
148 cyclones on ocean chlorophyll concentration, primarily using Bio-Argo floats. In contrast, our  
149 study offers a new perspective by utilizing subsurface profiles of a broader suite of  
150 biogeochemical variables, including chlorophyll, phytoplankton, nutrients, and oxygen  
151 concentration, complemented by multiple ocean satellite and reanalysis products. To date, such  
152 a comprehensive assessment has rarely been reported for the Mediterranean Sea. Here, we  
153 investigate the impact of Medicane Daniel on ocean biogeochemistry in the context of the SST  
154 anomalies along its path.

155

156 In this study, we highlight the co-occurrence of compound extreme events in the region prior  
157 to medicane Daniel's landfall. Specifically, we show that the intensification of medicane Daniel  
158 may have been driven by the combined influence of a WCE and an MHW. We examine the  
159 key atmospheric and oceanic factors that contributed to Daniel's development, ultimately  
160 making it one of the deadliest cyclones in the MS. The analysis also covers the critical role of  
161 the SWOT satellite in advancing air-sea interaction research; this is the first study to report the  
162 importance of SWOT data for air-sea interaction in the MS. Additionally, we investigate the  
163 medicane's impact on ocean biogeochemistry at the WCE location, providing insights into the  
164 underlying physical and biological processes that govern such interactions.

165

166 **2. Medicane Daniel Synoptic Overview and Intensification:** Daniel was formed in the MS  
167 from 4 to 12 September 2023. It was the deadliest cyclone in the Mediterranean basin during



168 the satellite era. The cyclone originated from an upper-level cut-off low and brought  
169 exceptionally heavy rainfall to Greece and Libya, triggering severe floods and mudslides.  
170 These catastrophic events led to at least 5,898 fatalities in Libya (HérinCs, 2023; Normand et  
171 al., 2024). On September 2-3, a swift cold front traversed Central Europe, generating an upper-  
172 level trough that created a cut-off low near Greece by September 4. Named "Daniel" by the  
173 Hellenic National Weather Service, this cyclone brought severe thunderstorms to Greece,  
174 Turkey, and Bulgaria due to unstable atmospheric conditions and warm waters. Moving south-  
175 southwest, it stalled over the Central Mediterranean, evolving into a subtropical storm by  
176 September 7. By September 9, Daniel transitioned into a tropical-like storm, making landfall  
177 in Libya on September 10, causing catastrophic floods. Daniel dissipated into a low-pressure  
178 trough by September 12 (HérinCs, 2023; Normand et al., 2024). Storm Daniel brought intense  
179 winds of up to 120 km/h and delivered a total of 240 mm of rainfall over a 25-hour period  
180 (Normand et al., 2024). It caused catastrophic flash flooding in Derna on September 10, 2023,  
181 as torrential rains overwhelmed the river's delta outlet. The flood destroyed large parts of the  
182 city's buildings, infrastructure, and bridges, resulting in 8.8 million tons of debris. In Derna  
183 alone, 10% of houses were destroyed and 18.5% damaged. In other cities, such as Susah,  
184 approximately 28% of homes were destroyed, while Albayda, Al-Marj, and others also suffered  
185 heavy losses. Overall, the storm led to 5,898 deaths, 8,000 missing persons, 44,800 displaced  
186 individuals, and 18,838 homes damaged across Libya's northeastern coast, making it the  
187 deadliest African storm since 1900 (Normand et al., 2024; Katsanos et al., 2024).  
188

### 189 **3. Data and Methods:**

#### 190 **3.1 Data sources and products used:**

191 In this study, the best-track data for the medicane Daniel was obtained from the Zivipotty  
192 Cyclone Report database (<https://zivipotty.hu/tcr.html>). Eddy identification was based on daily  
193 SLA fields sourced from the CMEMS. Specifically, the dataset  
194 SEALEVEL\_EUR\_PHY\_L4\_NRT\_OBSERVATIONS\_008\_060, with a spatial resolution of  
195 0.125°, was utilized. To detect and characterize the MHW, daily SST data from the NOAA  
196 Optimum Interpolation SST V2 dataset (Reynolds et al., 2007) were used. This dataset has a  
197 spatial resolution of 0.25° and covers the period from 1981 to the present. The key atmospheric  
198 variables, including total column water vapor (which represents the sum of water vapor, liquid  
199 water, cloud ice, rain, and snow in a column extending from the surface of the Earth to the top  
200 of the atmosphere), total precipitation (TP), vertical integrated moisture divergence (VIMD),  
201 mean sea level pressure (MSLP), and 10-meter zonal and meridional wind components, daily



202 radiative fluxes of shortwave and longwave radiations, (denoted as  $Q_{\text{SW}}$  and  $Q_{\text{LW}}$  respectively),  
 203 turbulent heat fluxes of latent and sensible flux (denoted as  $Q_{\text{lat}}$  and  $Q_{\text{sen}}$  respectively) were  
 204 retrieved from the ERA5 reanalysis (Hersbach et al., 2020). The surface net heat flux ( $Q_{\text{net}}$ )  
 205 was derived from a combination of radiative and turbulent fluxes (Menna et al., 2023).

207

208 High-resolution SLA observations were obtained from the SWOT Level 3 satellite product,  
209 which offers 2 km spatial resolution, provided by Archiving, Validation and Interpretation of  
210 Satellite Oceanographic data (AVISO; <https://www.aviso.altimetry.fr/en/data/products/sea->  
211 [surface-height-products/global/swot-l3-ocean-products.html](https://www.aviso.altimetry.fr/en/data/products/global/swot-l3-ocean-products.html)).

212 Lastly, biogeochemical parameters such as chlorophyll, phytoplankton, nutrients, and  
213 dissolved oxygen were accessed via the CMEMS from the product  
214 [MEDSEA MULTIYEAR BGC 006 008](#), available at a 4-5 km spatial resolution, and 1-hr  
215 temporal resolution (215)  
216 [https://doi.org/10.25423/cmcc/medsea\\_multiyear\\_bgc\\_006\\_008\\_medbfm3](https://doi.org/10.25423/cmcc/medsea_multiyear_bgc_006_008_medbfm3)). Daily satellite  
217 chlorophyll products with 1 km spatial resolution have also been used in this study (Volpe et  
218 al., 2019; Volpe et al., 2018; Berthon et al., 2004), which are archived from Copernicus  
219 (<https://doi.org/10.48670/moi-00298>).

220

221 **3.2 Methods:** In this study, we investigate medicare Daniel. A detailed description of the  
222 event and the methodologies employed in the analysis are provided below.

223

### 3.2.1 Eddy and Marine Heat Wave (MHW) identification:

225 Eddy identification in this study followed the approach of Jangir et al. (2021, 2023) and Sun et  
 226 al. (2017), based on geostrophic balance equations relating SLA to geostrophic currents. Zonal  
 227 (u) and Meridional (v) velocity components were derived using equations 2, 3, and 4:

231

232 where  $u$  and  $v$  are the zonal and meridional components,  $g$  is the acceleration caused by  
 233 gravity,  $f$  is the Coriolis parameter,  $h$  is the SLA, and  $V$  is the geostrophic current speed.



234

235 Eddies were classified by analysing flow circulation and SLA patterns: anti-cyclonic  
236 circulation with a local SLA maximum indicated WCEs, while cyclonic circulation with a local  
237 SLA minimum indicated cold-core eddies (CCEs). This is consistent with previous findings,  
238 where WCEs in the Northern Hemisphere exhibited clockwise (anti-cyclonic) rotation, while  
239 CCEs rotated counterclockwise (cyclonic). The relation between anti-cyclonic eddies and  
240 WCEs along the cyclone's path was also verified by inspecting SST anomalies with respect to  
241 a boxcar average.

242

243 MHWs were identified using the definition by Hobday et al. (2016) and the software developed  
 244 by Zhao et al. (2019) ([https://github.com/ZijieZhaoMMHW/m\\_mhw1.0](https://github.com/ZijieZhaoMMHW/m_mhw1.0)). An MHW is defined  
 245 as a period of at least five consecutive days during which the daily SST exceeds the seasonally  
 246 varying 90<sup>th</sup> percentile, based on a climatological reference period (1983–2021). Events  
 247 separated by less than three days are treated as a single MHW. Daily SST anomalies were  
 248 computed by subtracting the daily climatology. MHW intensity was classified following  
 249 Hobday et al. (2018) into four categories based on the metric  $\theta$  moderate ( $1 \leq \theta \leq 2$ ), strong  
 250 ( $2 < \theta < 3$ ), severe ( $3 < \theta < 4$ ), and extreme ( $\theta \geq 4$ ).

251 Where

### 253 3.2.2 Computation of Ocean Heat Content

254 We have also calculated the OHC to assess the role of subsurface heat accumulation in driving  
255 compound extreme events, such as the co-occurrence of MHWs and cyclones. Since the ocean  
256 acts as a key energy source for cyclones by supplying heat and moisture, the passage of a  
257 cyclone typically extracts heat from the upper ocean, leading to a decrease in OHC. In this  
258 study, OHC is defined as the vertically integrated thermal energy from the surface down to the  
259 depth of the 20 °C isotherm (a proxy for the thermocline layer). The OHC was computed for  
260 the medicane using the following formulation (Equation 6):

262 where  $\rho$  is the density of the seawater,  $C_p$  is the specific heat capacity of the seawater at  
 263 constant pressure,  $p$ ,  $h1$  is the surface,  $h2$  is the bottom depth, and  $T$  is the temperature in °C.

264 This approach allows us to quantify how much thermal energy is available in the upper ocean  
265 to potentially intensify cyclones and how this energy is depleted following cyclone passage.

### 266 3.2.3 Computation of Ekman pumping

Ekman pumping was computed using the wind stress components  $\tau = (\tau_x, \tau_y)$  from ERA5, namely Eastward Wind Stress (EWSS) and Northward Wind Stress (NSSS). To compute the wind stress curl ( $\nabla \times \tau$ ), the spatial derivatives of wind stress are used, and it is computed using equation 7:

272

273 Then, the Ekman pumping velocity ( $w_e$ ), introduced by Stern (1965) to account for the effect  
274 of the ocean currents on upwelling, is calculated using equation 8:

276 This vertical velocity reflects the upwelling (positive  $w_e$ ) or downwelling (negative  $w_e$ ) of  
 277 water, and is a crucial mechanism through which cyclones influence oceanic nutrient transport,  
 278 mixing, and biological productivity. Here, the relative vorticity ( $\zeta$ ) was computed from the  
 279 zonal ( $u$ ) and meridional ( $v$ ) components of the surface current, as given in Equation (9):

281

282 The Ekman transport vector components were computed from the wind stress and Coriolis  
283 parameter as:

286

287 where  $\rho$  is seawater density, and  $f$  is the Coriolis parameter (dependent on latitude). The vector  
 288 field  $\mathbf{M}=(M_x, M_y)$  was visualized using quiver plots to reveal the spatial structure and  
 289 directional response of Ekman transport to cyclone wind forcing.

290

## 291 4. Results and Discussion

292 *4.1 The presence of ocean features i.e., Eddies, Marine Heat Wave and Ocean Heat Content*  
293 *along the cyclone track and their Impact on cyclone intensity*



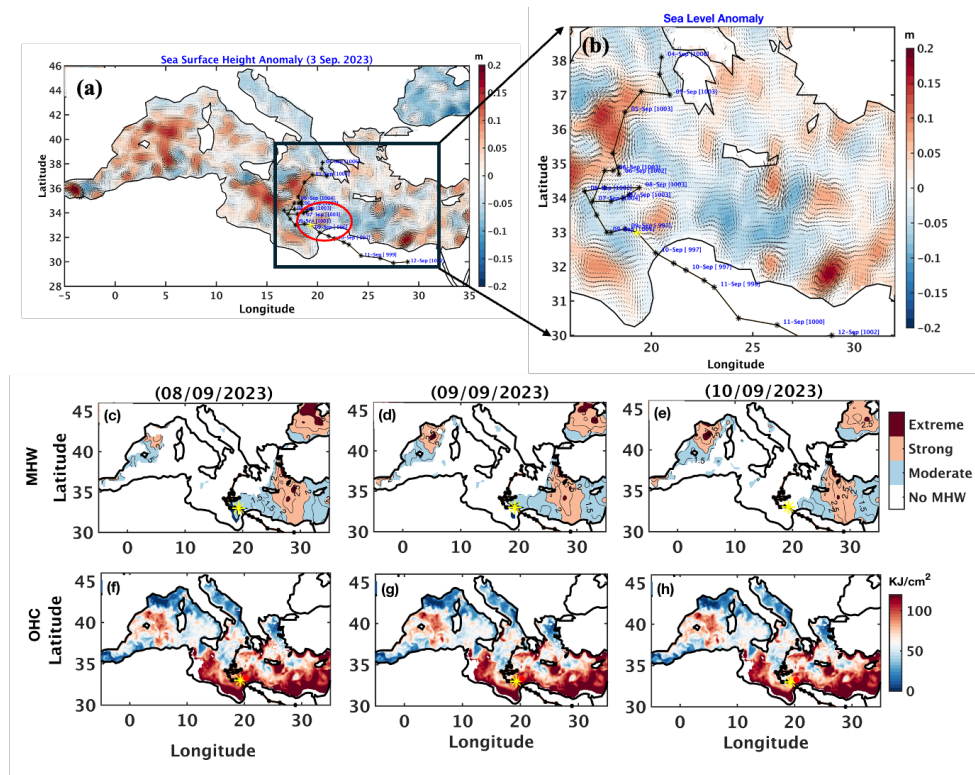
294 Figure 1a, b shows the SLA along the cyclone's track. At first, the medicane passed over a  
295 cluster of three anti-cyclonic WCEs between September 4 and 6, presumably contributing to  
296 its intensification (Jangir et al., 2023). This intensification is also supported by the presence of  
297 a MHW, as shown in Figure 1c–e (SI Figure 1), which reveals a moderate MHW at the  
298 intensification location on 9 September 2023. The presence of two extreme conditions, namely  
299 the WCE and MHW, at the intensification site near the coastal region may have contributed to  
300 making this the deadliest cyclone recorded in the MS (Figure 1). Rathore et al. (2022) and  
301 Jangir et al. (2024) highlighted the critical role of sudden intensification in Cyclone Amphan  
302 over the Indian Ocean and medicane Ianos over the MS, respectively, in the presence of MHWs  
303 along their paths. The findings of the current study are consistent with these observations,  
304 demonstrating that while cyclone genesis and intensification can occur independently of such  
305 features, the presence of WCEs and MHWs can significantly enhance the rate and magnitude  
306 of intensification over a shorter time.

307 Figures 1 mainly highlights the potential importance of ocean characteristics such as WCEs  
308 and MHWs in cyclone intensification, indicating that cyclone intensity increased in the  
309 presence of WCEs and MHWs. This behavior is similar to how cyclones in other ocean basins  
310 react to changes in intensification factors related to underlying eddies (Ali et al., 2007; Lin et  
311 al., 2013; Jangir et al., 2020; Jangir et al., 2023). When a cyclone encounters a WCE, the  
312 negative feedback loop between cyclone intensity and SST diminishes. Normally, cyclones  
313 absorb heat from the ocean, causing surface cooling through mixing and evaporation, reducing  
314 their intensity. However, if a WCE or MHW is present, the high SST persists longer,  
315 intensifying the cyclone and reducing the negative feedback effect (Bender et al., 1993; Jangir  
316 et al., 2024).

317 Furthermore, Cyclones also draw a significant portion of their energy from warm, deep ocean  
318 waters; therefore, quantifying the amount of this warm, deep water provides a more accurate  
319 measure of the energy available to the storm. OHC serves as this metric, indicating how much  
320 warm water a cyclone can convert into energy. Studies have shown that OHC is a far superior  
321 predictor compared to SST alone (Wada & Usui, 2007; Sharma and Ali, 2014; Lin et al., 2013;  
322 Law et al., 2011). Analysis of the OHC revealed that there is a significant amount of OHC at  
323 the intensification locations, providing the energy necessary for medicane Daniel to intensify.  
324 Approximately 120 KJ/cm<sup>2</sup> of heat was available from September 4<sup>th</sup> to 9<sup>th</sup>, even before the  
325 cyclone's intensification (Figure 1f-h & SI Figure 2). This accumulated heat at the



327 intensification location is attributed to the presence of the eddy and the MHW, which decreases  
328 after the passage of the medicane on the 11<sup>th</sup> and 12<sup>th</sup> of September, 2023 (SI Figure 2). The  
329 presence of the accumulated heat in the form of OHC maintains intensity by reducing negative  
330 feedback that occurs due to the passage of the cyclone (Jangir et al., 2023; Jangir et al., 2024).



331

332 *Figure 1: (a, b) Sea level anomaly in shading and geostrophic currents arrows, Medicane track  
333 overlaid on (c,e) Marine Heat Wave and (f,h) Ocean Heat Content, Yellow star represents the  
334 intensification location and the red dot on Ocean Heat Content showing the location of WCE.*  
335

#### 336 **4.2 The role of Atmospheric Precursors in the Intensification of Medicane Daniel**

337 The MSLP, wind speed (WS), and net heat flux (NHF) along the cyclone's track are shown in  
338 Figure 2a. The MSLP, computed using the Cressman averaging method (Cressman, 1959),  
339 indicates moderate intensification when the storm passes over the WCE on 5 September (Figure  
340 2a). Subsequently, from the 6th to the 7th, the medicane passes over a CCE region, and its  
341 intensity is reduced. Upon reaching the vicinity of Libya's coast on the 8th, it quickly  
342 intensifies. An additional WCE was present in the vicinity of the cyclone's path at that time,

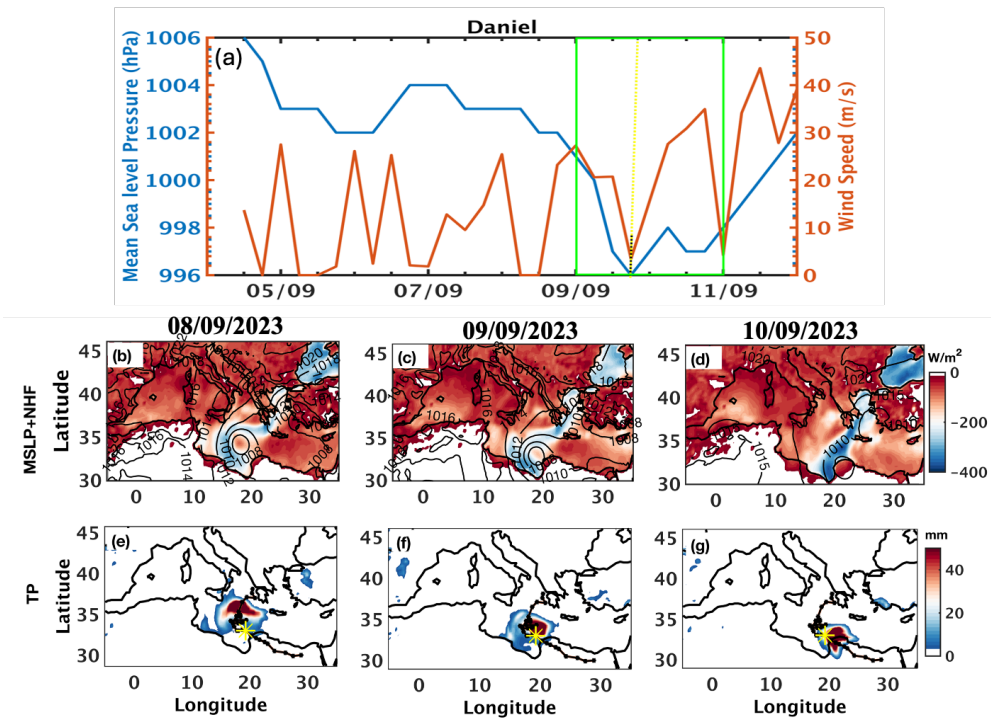


343 potentially further contributing to its fast intensification. This fast intensification is indicated  
344 by a drop in the MSLP and a sudden increase in WS near the eddy and MHW location (Figure  
345 2a). Figure 2a shows that on September 7, 2023, the MSLP was 1003 hPa. Upon reaching the  
346 vicinity of the eddy, the MSLP dropped by 6 hPa to 997 hPa (Figure 2a) in 12 hours, and  
347 significant NHF were released at the cyclone's intensification location (Figure 2b-d and SI  
348 Figure 3), providing the energy necessary for the cyclone to intensify. The cutoff low persisted  
349 for two days (Figures 2b-d, SI Figure 3), even after the cyclone made landfall in Libya,  
350 resulting in significant damage along the Libyan coast.

351 Moisture processes play an equally important role in cyclone intensification. Their significance  
352 has been demonstrated in previous studies by Jangir et al. (2023) and Pytharoulis et al. (2018),  
353 emphasizing that elevated SST in the form of eddy or MHW is essential in providing moisture  
354 to a medicane via surface fluxes, enhancing convection. Additionally, Jangir et al. (2024)  
355 highlighted the importance of moisture convergence in the intensification of cyclones and  
356 increasing total associated precipitation. Thus, motivated by these findings, in this study we  
357 mainly focus on the cause of the intensification of the medicane Daniel and the extreme flood  
358 that occurred during the event.

359 The analysis of moisture convergence (i.e., mean vertically integrated moisture divergence)  
360 showed a pattern of moisture convergence along the cyclone's path. Notably, this convergence  
361 coincides with the eddy location at the intensification location on September 9th, 2023 (SI  
362 Figure 4). This alignment suggests that the eddy supplied the moisture needed for the cyclone's  
363 intensification. The interaction between the eddy and the medicane likely enhanced moisture  
364 availability, contributing to the storm's strengthening at that specific point in its path.  
365 Additionally, the total column water was notably high at the eddy and MHW locations. While  
366 this total water was present before the intensification location as well, it converged around the  
367 eddy at the intensification location (SI Figure 5), leading to substantial precipitation in that area  
368 (Figure 2e-g and SI Figure 6). The severe precipitation near the coastal region, primarily due  
369 to the presence of a WCE and MHW, significantly contributed to the extensive destruction  
370 along the Libyan coast. The WCE's influence intensified the cyclone by providing additional  
371 moisture and heat, leading to heavy rainfall. This heavy precipitation, concentrated near the  
372 coast, exacerbated the storm's impact, severely damaging the affected areas.

373  
374  
375



376

377 *Figure: 2(a) Mean sea level pressure, wind speed, and net heat flux computed using the*  
378 *Cressman average along the track of the medicane Daniel. Medicane track overlaid on (b-d)*  
379 *Contours of the daily mean of MSLP overlaid on the daily mean of latent heat fluxes (positive*  
380 *downward), and (e-g) total precipitation during the cyclone, on the 8th, 9th and 10th September*  
381 *2023. Yellow star represents the intensification location.*

382

#### 383 **4.3 Use of SWOT satellite data in cyclone studies in the Mediterranean Sea**

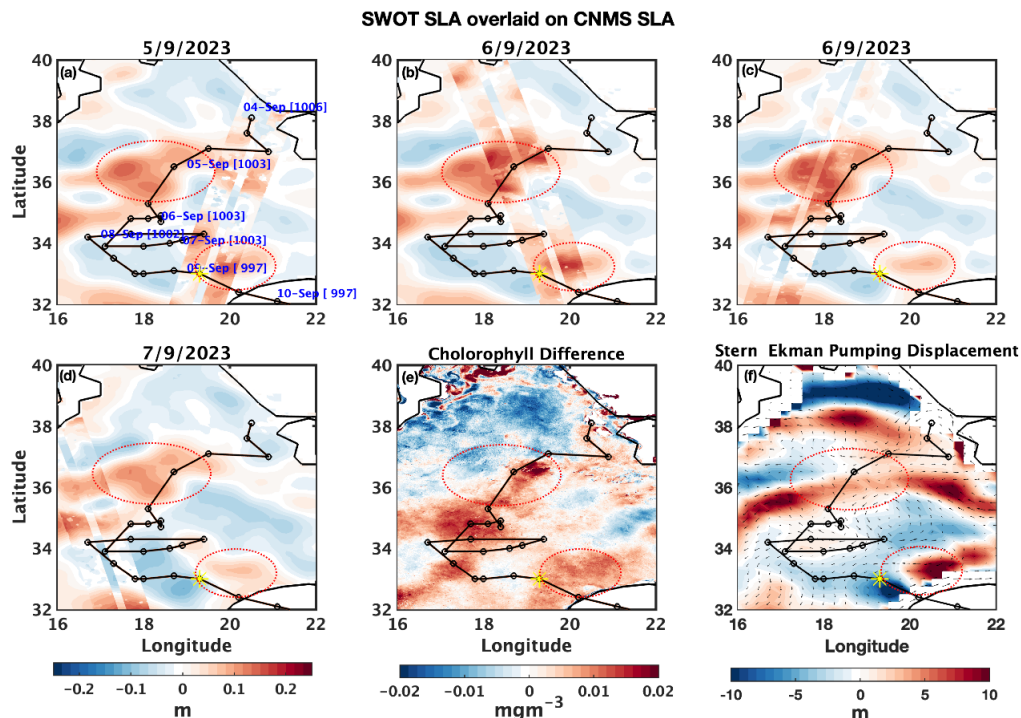
384 The SWOT mission offers high-resolution sea surface height anomaly (SSHA) or SLA data  
385 with unprecedented spatial detail, enabling precise detection of mesoscale and sub-mesoscale  
386 ocean features, such as eddies and fronts (Morrow et al., 2019). This can be valuable for  
387 studying cyclones, which interact strongly with oceanic eddies that influence storm intensity.  
388 Unlike traditional altimeters, SWOT's wide-swath coverage captures fine-scale structures  
389 generated by cyclone-induced mixing.

390

391 Here we show the SWOT swath passing over the location of the eddies along the track of  
392 medicane Daniel (Figure 3). In Figures 3a and 3b, the eddy initially appears small and low  
393 intensity in the CMEMS, and the cyclone is observed nearby. However, SWOT data reveals a



394 more intense and extensive eddy structure with the cyclone positioned directly above it.  
395 Notably, Figure 3e shows a high post-cyclone increase in Chl-a concentration over both the  
396 eddy locations. Complementary to this, Figure 3 indicates enhanced Ekman pumping roughly  
397 at the same locations, likely contributing to the observed Chl-a increment over both eddies.  
398 These findings report the value of SWOT observations in capturing fine-scale oceanic features  
399 and dynamics, offering critical insights into cyclone-eddy interactions, vertical nutrient  
400 transport, investigating sub-mesoscale air-sea interactions, and improving coupled ocean-  
401 atmosphere models.



402  
403 *Figure 3: (a-d) The SWOT SLA swath (with resolution 2 km) overlaid on SLA from CMEMS*  
404 *(12.5 km spatial resolution). (e) Satellite chlorophyll (2 km spatial resolution) before and after*  
405 *Storm Daniel. (f) Average (5-10 September 2023) Ekman pumping displacement and arrows*  
406 *of transport vector during the cyclone.*

407

#### 408 **4.4 Impact of medicane Daniel on ocean biogeochemistry**

409 To investigate the impact of the medicane on oceanic physical and biogeochemical properties,  
410 we analyzed vertical profiles of key variables along the cyclone's track. The analysis focused  
411 on differences between two days after the cyclone's passage minus two days before (Figure  
412 4a-g). The results reveal a notable decrease in temperature along the cyclone path, with the



413 strongest cooling observed near the WCE and MHW locations. In contrast, Chl-a and  
414 phytoplankton concentrations at the surface exhibit a marked dipole at the subsurface. This  
415 biological response is attributed to cyclone-induced upwelling and vertical mixing. Enhanced  
416 nutrient availability at the subsurface layer allows for sufficient sunlight, and together with  
417 elevated oxygen concentrations, may foster increased surface Chl-a and phytoplankton  
418 biomass. Signs of this can be seen in the MHW region, where higher Chl-a concentrations  
419 reach the surface. But, unlike previous results ([Jangir et al., 2026](#)), medicane Daniel only shows  
420 a small increase in Chl-a at the surface in the MHW region. Profiles of temperature and Chl-a  
421 at the maximum cyclone intensity location and time (Figure 4h, i) reveal that the DCM was  
422 located far below the MLD, at around 140m depth. We already know that cyclone-induced  
423 upwelling was negative there (Figure 3f), indicating downwelling, so it cannot explain the  
424 increase in Chl-a at the surface. The profiles in Figure 4i are in agreement with the  
425 downwelling, showing a small decrease in the DCM depth. The subsurface crossings between  
426 the profiles in this figure indicate that a different mechanism was active, that is, cyclone-  
427 induced subsurface mixing. This mechanism is typically slower than turbulence in the mixed  
428 layer, but under storm conditions may become comparable. The gradual subsurface increase in  
429 Chl-a, as opposed to the vertical line observed in the mixed layer, suggests that subsurface  
430 turbulence is comparable to, but still weaker than, turbulence within the mixed layer.

431

432 To further investigate the underlying mechanisms, vertical cross-sections over the main WCE  
433 region were analyzed during the pre-storm, during storm, and post-storm phases (Figure 5).  
434 These sections reveal notable eddy-dependent subsurface changes associated with the passage  
435 of the medicane. As expected, during and after the passage of the storm, significant surface  
436 cooling is observed (panels b-d and h-i). In addition to the cooling observed within the mixed  
437 layer, three distinct circular-like cooling patterns are evident immediately beneath it. These  
438 may indicate a secondary circulation motion starting at the deep sub-surface (below 200m),  
439 which transfers deep cold water to the layers below the mixed layer. In this case, the two  
440 patterns on the right indicate an upwelling cell at the WCE boundaries and another at the CCE  
441 center. These circulation cells also create the Chl-a patterns of DCM upwelling inside the  
442 WCE, but they do not explain the dipole pattern above the WCE.

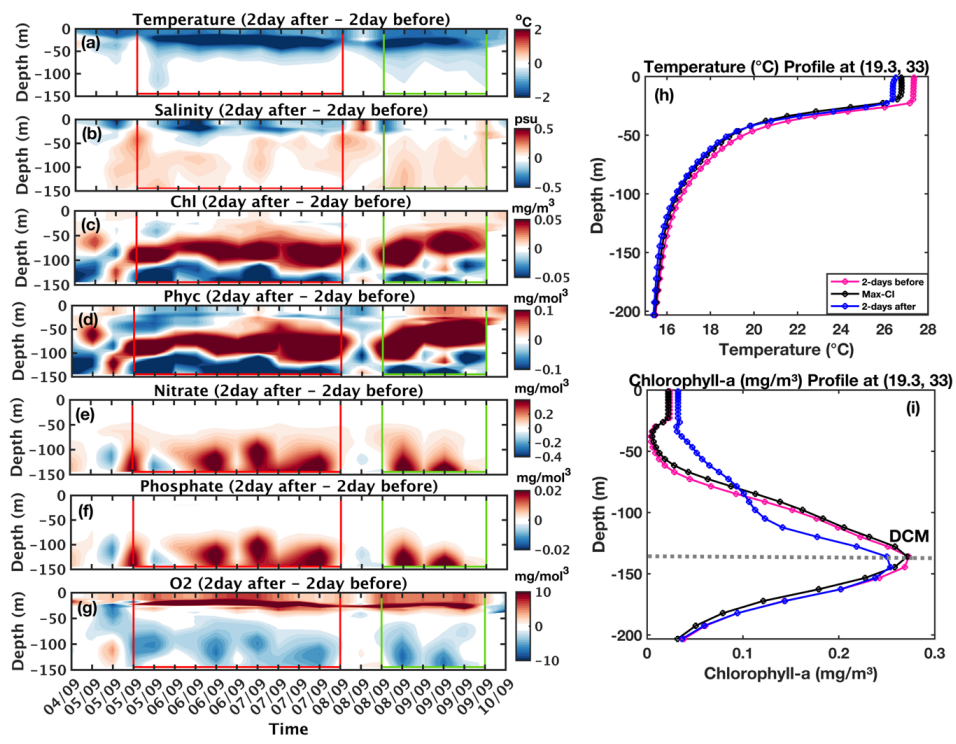
443

444 Figure 6 shows vertical profiles of Chl-a in two locations along the same line as in Figure 7a,  
445 one inside the CCE and one inside the WCE. These can guide us about the relevant active  
446 mechanisms. Inside the WCE, high Ekman pumping (Figure 3f) results in upwelling and



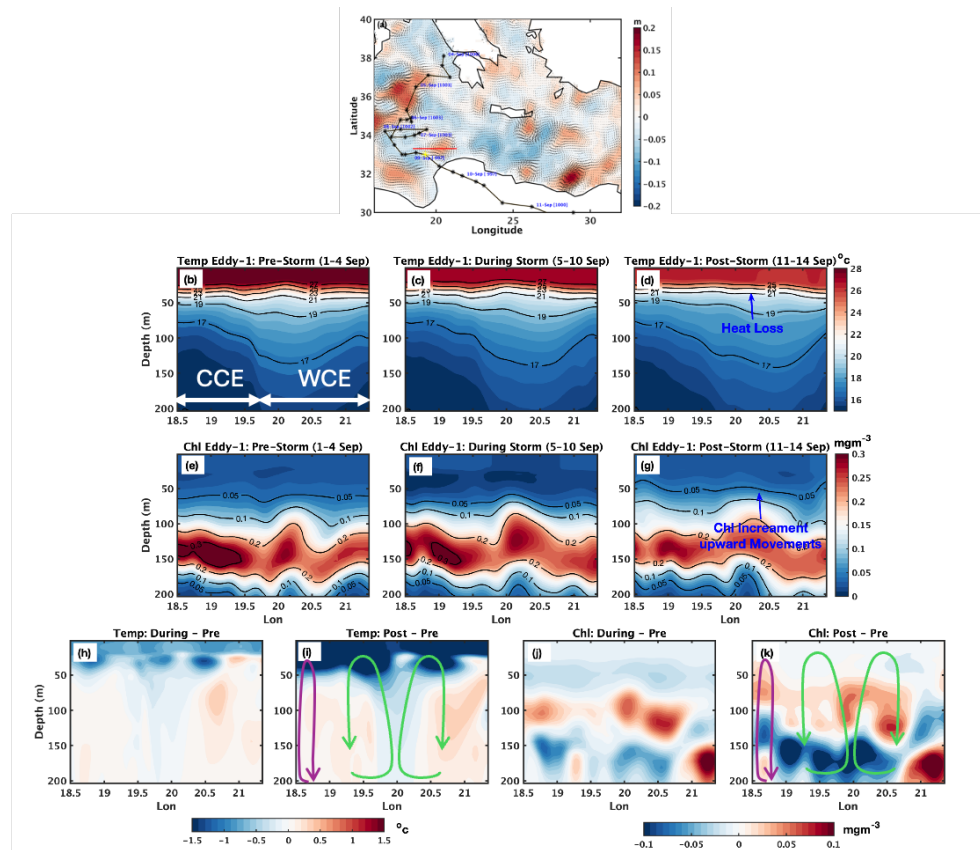
447 upward shift of the DCM depth. Inside the CCE, Ekman pumping is less relevant - the DCM  
 448 stays more or less at the same depth. Yet, the profiles in Figure 6a suggest that the dipole  
 449 patterns inside the CCE in Figure 5k can be explained by subsurface mixing, which is stronger  
 450 above the DCM. These observations suggest that although WCEs are generally associated with  
 451 downwelling and reduced biogeochemical activity, the strong mixing and upwelling induced  
 452 by the cyclone temporarily dominate this dynamic, leading to surface nutrient enrichment and  
 453 increased biological activity. In the CCE, although the Ekman pumping is smaller (or negative),  
 454 the higher DCM depth supports mixing of Chl-a to the surface through sub-surface mixing.

455



456

457 *Figure 4: Profile of physical (a-d) and biogeochemical variables (e-g) along the path of the*  
 458 *cyclone. The left panels represent the difference between two days after the event minus two*  
 459 *days before the event. The red and green vertical lines in panels a-g bound the location of*  
 460 *MHW and WCE along the track of the Mediterranean cyclone Daniel, respectively. The vertical*  
 461 *dotted black mark marks the location of the cyclone's maximum intensity.*



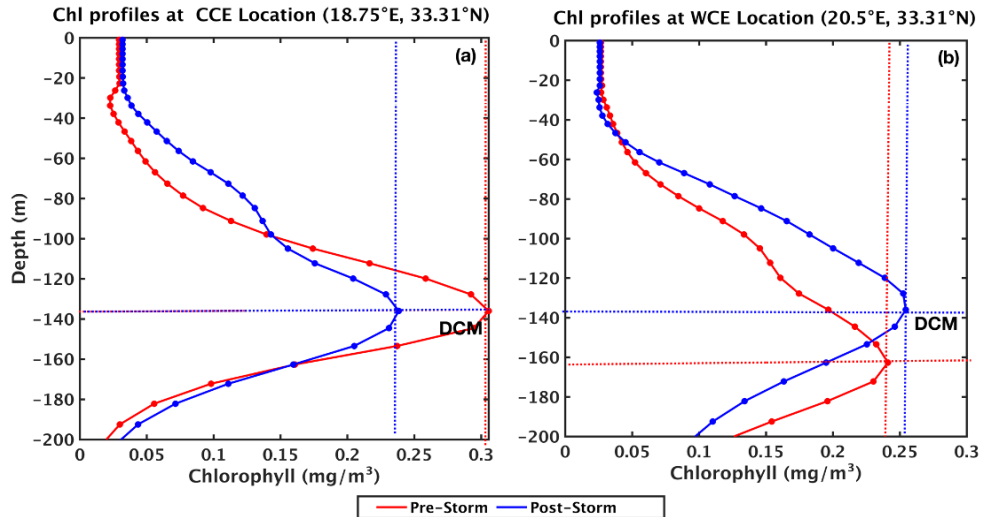
462

463 *Figure 5: (a) Sea level anomaly and a red line representing the section over the second WCE,*  
 464 *which is considered in the next panels. (b-d) Temperature profiles and isotherms before,*  
 465 *during, and after the medicane along the section over the eddy. (e-g) Chlorophyll profiles*  
 466 *before, during, and after the medicane along the section over the eddy. (h-i) The difference in*  
 467 *temp during-storm minus pre-storm and post-storm minus pre-storm. (j-k) are the same as (h-)*  
 468 *j) for Chl-a. Green arrows represent the estimated location of a secondary circulation cell, and*  
 469 *the purple arrow indicates subsurface mixing.*

470

471

472



473

474 *Figure 6: The Chlorophyll profiles before the storm (1–4 September), and after the storm (11–*

475 *14 September) at the CCE location and WCE location.*

476

## 477 5. Conclusions

478 This study has provided comprehensive insights into the intensification and impact of the  
479 medicane Daniel, which formed in the MS in September 2023. The findings show the  
480 significant role of oceanic and atmospheric variables in cyclone intensification, particularly the  
481 presence of WCE and MHW (Figure 7). These oceanic features reduced the negative feedback  
482 loop between cyclone intensity and SST, allowing the cyclone to maintain and even increase  
483 its intensity. This study also highlighted the importance of OHC in providing the energy  
484 necessary for cyclone intensification, with approximately 120 KJ/cm<sup>2</sup> of heat available at the  
485 intensification location over the WCE and MHW. Additionally, the convergence of moisture  
486 at the locations of the WCE and MHW, combined with the elevated total water column,  
487 contributed to the heavy precipitation observed in the coastal areas in Libya.

488

489 This study highlights the critical role of high-resolution SWOT data in advancing our  
490 understanding of air-sea interaction processes. While CMEMS data, with its coarser spatial  
491 resolution, suggests the presence of a weak eddy near the cyclone intensification region,  
492 SWOT's finer 2 km resolution reveals a high-intensity WCE precisely aligned with the  
493 cyclone's path. This enhanced detection capability provides a more accurate illustration of eddy  
494 characteristics and their influence on cyclone dynamics. Furthermore, satellite-derived Chl-a  
495 data indicate an enhanced bloom over the WCE location, supported by positive Ekman



496 pumping values. These high values indicate cyclone-induced upward movement of water from  
497 deeper layers to the surface, bringing cold, nutrient-rich water to the surface, and boosting  
498 ocean productivity.

499

500 Subsurface profiles of physical and biogeochemical properties show a notable temperature  
501 decrease above the mixed layer depth, particularly over the WCE and MHW regions. The  
502 passage of the cyclone triggers vertical mixing, leading to an increase in surface nutrient  
503 concentrations. Combined with sufficient sunlight in the euphotic zone, this promotes a surge  
504 in surface Chl-a and phytoplankton productivity. Cross-sectional analysis further reinforces  
505 these findings: a clear upward shift in isotherms following the cyclone indicates heat loss and  
506 active upwelling over the WCE. Concurrently, the chlorophyll sections display an upward  
507 displacement and intensification of chlorophyll concentrations, confirming the strong  
508 biogeochemical response induced by the cyclone's passage over the WCE region.

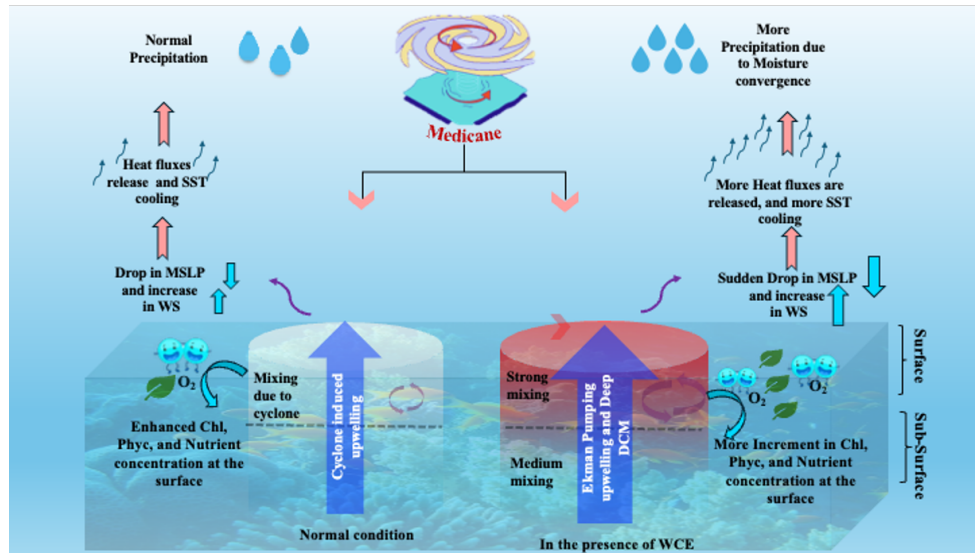
509

510 In conclusion, the study of medicane Daniel emphasizes the need for a deeper understanding  
511 of both oceanic and atmospheric factors in predicting and mitigating the impacts of such  
512 cyclones in the MR. The findings suggest that, similar to tropical cyclones in other ocean  
513 basins, medicanes are strongly influenced by the interplay of oceanic heat content, eddies, and  
514 atmospheric dynamics, which together determine the intensity and destructiveness of these  
515 storms.

516

517

518



519  
520 *Figure 7: Schematic of the process responsible for the cyclone intensification over eddy and*  
521 *MHW and their impact on ocean biogeochemistry*

522

523

#### 524 **Data Availability:**

525

526 Data can be Archived from the links below-

527 [https://doi.org/10.25423/cmcc/medsea\\_multiyear\\_bgc\\_006\\_008\\_medbfm3](https://doi.org/10.25423/cmcc/medsea_multiyear_bgc_006_008_medbfm3)

528

529

530

#### 531 **Author Contributions:**

532

533 B.J. contributed to the conceptualization of the study, data curation, formal analysis, and writing of the original draft.

534

535 E.S. served as the project investigator, contributed to conceptualization, provided resources  
536 and software support, supervised the research, and contributed to writing, review, and editing,  
537 as well as funding acquisition.

538

539

**Competing Interests:** The authors declare no conflict of interest.

540

**Acknowledgments:** The authors acknowledge the data-providing agencies (i.e., CMEMS, AVISO) for providing data free of cost.

542

**Funding:** This research was supported by the Israel Science Foundation (Grant 2228/21).

543

544

#### **References**



545 Ali, M. M., Jagadeesh, P. S. V. and Jain, S., 2007. Effects of eddies on Bay of Bengal cyclone intensity,  
546 *Eos Trans. AGU*, 88(8), 93–95, doi:[10.1029/2007EO080001](https://doi.org/10.1029/2007EO080001).

547

548 Archer, M., Wang, J., Klein, P. *et al.*, 2025. Wide-swath satellite altimetry unveils global submesoscale  
549 ocean dynamics. *Nature* 640, 691–696. <https://doi.org/10.1038/s41586-025-08722-8>

550

551 Avolio, E., Fanelli, C., Pisano, A., & Miglietta, M. M. 2024. Unveiling the relationship between  
552 Mediterranean tropical-like cyclones and rising Sea Surface Temperature. *Geophysical Research  
553 Letters*, 51, e2024GL109921. <https://doi.org/10.1029/2024GL109921>

554

555 Bender, M. A., Ginis, I., and Kurihara, Y., 1993. Numerical simulations of tropical cyclone-ocean  
556 interaction with a high-resolution coupled model, *J. Geophys. Res.*, 98(D12), 23245–23263,  
557 doi:[10.1029/93JD02370](https://doi.org/10.1029/93JD02370).

558

559 Berthon, J.-F., Zibordi, G., 2004. Bio-optical relationships for the northern Adriatic Sea. *Int. J. Remote  
560 Sens.*, 25, 1527–1532.

561

562 Chen, Y., Pan, G., Mortimer, R., Zhao, H., 2022. Possible Mechanism of Phytoplankton Blooms at the  
563 Sea Surface after Tropical Cyclones. *Remote Sensing*, 14, 6207. doi: 10.3390/rs14246207

564

565 Cherif, S., Doblas-Miranda, E., Lionello, P., Borrego, C., Giorgi, F., Iglesias, A., *et al.*, 2020. Drivers of  
566 change. In *Climate and environmental change in the Mediterranean Basin—current situation and risks  
567 for the future* (pp. 59–128). First Mediterranean Assessment Report. Union for the Mediterranean, Plan  
568 Bleu, UNEP/MAP.

569

570 Chowdhury, R. R., Prasanna Kumar, S., Narvekar, J., & Chakraborty, A., 2020. Back-to-back  
571 occurrence of tropical cyclones in the Arabian Sea during October–November 2015: Causes and  
572 responses. *Journal of Geophysical Research: Oceans*, 125, e2019JC015836. doi:  
573 [10.1029/e2019JC015836](https://doi.org/10.1029/e2019JC015836)

574

575 Claud, C., Alhammoud, B., Funatsu, B. M., and Chaboureau, J.-P., 2010. Mediterranean hurricanes:  
576 large-scale environment and convective and precipitating areas from satellite microwave observations,  
577 *Nat. Hazards Earth Syst. Sci.*, 10, 2199–2213, <https://doi.org/10.5194/nhess-10-2199-2010>.

578

579 Cressman, G. P., 1959. An operational objective analysis scheme. *Monthly Weather  
580 Review*, 87, 367–374. doi: [10.1175/1520-0493\(1959\)087<0367:aoaos>2.0.co;2](https://doi.org/10.1175/1520-0493(1959)087<0367:aoaos>2.0.co;2)

581

582 Dutta, D., Mani, B. & Dash, M.K., 2019. Dynamic and thermodynamic upper-ocean response to the  
583 passage of Bay of Bengal cyclones ‘Phailin’ and ‘Hudhud’: a study using a coupled modelling system.  
584 *Environ Monit Assess* 191 (Suppl 3), 808.. <https://doi.org/10.1007/s10661-019-7704-9>.

585

586 Emanuel, K., 2005. Genesis and maintenance of “Mediterranean hurricanes.” *Advances in Geosciences*,  
587 2, 217–220. <https://doi.org/10.5194/adgeo-2-217-2005>

588 Fita, L., Romero, R., Luque, A., Emanuel, K., and Ramis, C., (2007) Analysis of the environments of  
589 seven Mediterranean tropical-like storms using an axisymmetric, nonhydrostatic, cloud resolving  
590 model, *Nat. Hazards Earth Syst. Sci.*, 7, 41–56, <https://doi.org/10.5194/nhess-7-41-2007>.



591  
592 Flaounas, E., Raveh-Rubin, S., Wernli, H., Drobinski, P., and Bastin, S., (2015). The dynamical  
593 structure of intense Mediterranean cyclones, *Clim. Dynam.*, 44, 2411–2427,  
594 <https://doi.org/10.1007/s00382-014-2330-2>

595  
596 Flaounas, E.; Davolio, S.; Raveh-Rubin, S.; Pantillon, F.; Miglietta, M.M.; Gaertner, M.A.; Hatzaki,  
597 M.; Homar, V.; Khodayar, S.; Korres, G.; et al., 2022. Mediterranean Cyclones: Current Knowledge  
598 and Open Questions on Dynamics, Prediction, Climatology and Impacts. *Weather Clim. Dyn.* 3, 173–  
599 208

600  
601 Flaounas, E., Dafis, S., Davolio, S., Faranda, D., Ferrarin, C., Hartmuth, K., Hochman, A.,  
602 Koutroulis, A., Khodayar, S., Miglietta, M. M., Pantillon, F., Patlakas, P., Sprenger, M., and  
603 Thurnherr, I.: Dynamics, predictability, impacts and climate change considerations of the  
604 catastrophic Mediterranean Storm Daniel (2023), *Weather Clim. Dynam.*, 6, 1515–1538,  
605 <https://doi.org/10.5194/wcd-6-1515-2025>, 2025.

606  
607 Flocas, H. A., 2000. Diagnostics of cyclogenesis over the Aegean sea using potential vorticity inversion,  
608 *Meteorol. Atmos. Phys.*, 73, 25–33, <https://doi.org/10.1007/s007030050061>

609  
610 González-Alemán, J. J., Pascale, S., Gutierrez-Fernandez, J., Murakami, H., Gaertner, M. A., & Vecchi,  
611 G. A. (2019). Potential increase in hazard from Mediterranean hurricane activity with global warming.  
612 *Geophysical Research Letters*, 46, 1754–1764. <https://doi.org/10.1029/2018GL081253>

613  
614 Hersbach, H., Bell, B., Berrisford, P., Hirahara, S., Horanyi, A., Munoz-Sabat, J., et al., 2020. The  
615 Era5 global reanalysis. *Quarterly Journal of the Royal Meteorological Society*, 146, 1999–2049, doi:  
616 [10.1002/qj.3803](https://doi.org/10.1002/qj.3803).

617  
618 Hérinçs, D., 2023. *Tropical Storm Daniel: Mediterranean tropical cyclone report (7–10 September*  
619 *2023)*. Zivipoty.hu. [https://zivipoty.hu/2023\\_daniel.pdf](https://zivipoty.hu/2023_daniel.pdf)

620  
621 Hobday, A. et al., 2016. A hierarchical approach to defining marine heatwaves. *Prog. Oceanogr.* 141,  
622 227–238.

623  
624 Hobday, A.J., Oliver, E.C.J., Sen Gupta, A., Benthuyzen, J.A., Burrows, M.T., Donat, M.G., Holbrook,  
625 N.J., Moore, P.J., Thomsen, M.S., Wernberg, T., and Smale, D.A., 2018. Categorizing and naming  
626 marine heatwaves. *Oceanography* 31(2):162–173, <https://doi.org/10.5670/oceanog.2018.205>.

627  
628 Hochman, A., Scher, S., Quinting, J., Pinto, J. G., & Messori, G., 2021. A new view of heat wave  
629 dynamics and predictability over the eastern Mediterranean. *Earth System Dynamics*, 12(1), 133–149.  
630 <https://doi.org/10.5194/esd-12-133-2021>

631  
632 IPCC., 2021. In V. Masson-Delmotte, P. Zhai, A. Pirani, S. L. Connors, C. Péan, et al. (Eds.), *Climate*  
633 *Change 2021: The Physical Science Basis. Contribution of Working Group I to the Sixth Assessment*  
634 *Report of the Intergovernmental Panel on Climate Change*. Cambridge University Press.  
635 <https://doi.org/10.1017/9781009157896>

636



637 Jangir B., Mishra A. K., Strobach, E., 2024. The interplay between medicanes and the Mediterranean  
638 Sea in the presence of sea surface temperature anomalies, *Atmospheric Research*, Volume 310, 107625,  
639 ISSN 0169-8095, <https://doi.org/10.1016/j.atmosres.2024.107625>.

640

641 Jangir, B., Mishra, A. K., & Strobach, E., 2023. Effects of mesoscale eddies on the intensity of cyclones  
642 in the Mediterranean Sea. *Journal of Geophysical Research: Atmospheres*, 128, e2023JD038607, doi:  
643 [10.1029/2023JD038607](https://doi.org/10.1029/2023JD038607)

644

645 Jangir, B., Swain, D., & Ghose, S., 2021. Influence of eddies and tropical cyclone heat potential on  
646 intensity changes of tropical cyclones in the North Indian Ocean. *Advances in Space Research*, 68(2),  
647 773–786, doi: [10.1016/j.asr.2020.01.011](https://doi.org/10.1016/j.asr.2020.01.011)

648

649 Jangir, B., Reale, M., Menna, M., Mishra, A. K., Marellucci, R., Cossarini, G., et al. (2026). The  
650 response of the physical and biogeochemical marine environment to the passage of Mediterranean  
651 cyclones in the presence of eddies, gyres, and marine heat wave. *Journal of Geophysical Research: Oceans*, 131, e2025JC023151. <https://doi.org/10.1029/2025JC023151>

652

653

654 Katsanos, D., Retalis, A., Kalogiros, J., Psiloglou, B. E., Roukounakis, N., & Anagnostou, M., 2024.  
655 Performance Evaluation of Satellite Precipitation Products During Extreme Events—The Case of the  
656 Medicane Daniel in Thessaly, Greece. *Remote Sensing*, 16(22), 4216.  
657 <https://doi.org/10.3390/rs16224216>

658

659 Khodayar, S., Kushta, J., Catto, J. L., Dafis, S., Davolio, S., Ferrarin, C., et al., 2025. Mediterranean  
660 cyclones in a changing climate: A review on their socio-economic impacts. *Reviews of Geophysics*, 63,  
661 e2024RG000853. <https://doi.org/10.1029/2024RG000853>.

662

663 Kouroutzoglou, J., Flocas, H. A., Keay, K., Simmonds, I., and Hatzaki, M., 2011. Climatological  
664 aspects of explosive cyclones in the Mediterranean, *Int. J. Climatol.*, 31, 1785–1802,  
665 <https://doi.org/10.1002/joc.2203>.

666

667 Latha, P. T., Rao, K.H., Nagamani, P.V., Amminedu, E., Choudhury, S.B., Dutt, C.B.S. and Dadhwal,  
668 V.K., 2015. Impact of Cyclone PHAILIN on Chlorophyll-a Concentration and Productivity in the Bay  
669 of Bengal. *International Journal of Geosciences*, 6, 473-480, doi: [10.4236/ijg.2015.65037](https://doi.org/10.4236/ijg.2015.65037).

670

671 Law K., 2011. The Impact of Oceanic Heat Content on the Rapid Intensification of Atlantic Hurricanes,  
672 Chapter 17. In: Lupo, A., eds. *Recent Hurricane Research - Climate, Dynamics, and Societal Impacts*.  
673 Croatia : InTech: 331-354.

674

675 Lin, I. I., Goni, G. J., Knaff, J. A., ZForebas, C., Ali, M. M., 2013. Ocean heat content for tropical  
676 cyclone intensity forecasting and its impact on storm surge, *Nat. Hazards*, 66, pp. 1481-1500,  
677 10.1007/s11069-012-0214-5

678

679 Liu, Y., Tang, D., Tang, S., Morozov, E., Liang, W., Sui, Y., 2020. A case study of Chlorophyll a  
680 response to tropical cyclone Wind Pump considering Kuroshio invasion and air-sea heat exchange.  
681 *Science of Total Environment*, 741:140290. doi: [10.1016/j.scitotenv.2020.140290](https://doi.org/10.1016/j.scitotenv.2020.140290). Epub 2020 Jun 18.  
682 PMID: 32603939.

683



684 Ma, Z.,2018. Examining the contribution of surface sensible heat flux induced sensible heating to  
685 tropical cyclone intensification from the balance dynamics theory. *Dynamics of Atmospheres and*  
686 *Oceans*, 84, 33–45. <https://doi.org/10.1016/j.dynatmoce.2018.09.001>

687

688 MedECC.,2020. Climate and environmental change in the Mediterranean Basin—Current situation and  
689 risks for the future. In W. Cramer, J. Guiot, & K. Marini (Eds.), *First Mediterranean assessment report*,  
690 Union for the Mediterranean, Plan Bleu (p. 632). UNEP/MAP.

691

692 Menna, M., Martellucci, R., Reale, M. *et al.*,2023 A case study of impacts of an extreme weather system  
693 on the Mediterranean Sea circulation features: Medicane Apollo (2021). *Scintific Report*, 13, 3870, doi:  
694 [10.1038/s41598-023-29942-w](https://doi.org/10.1038/s41598-023-29942-w).

695

696 Miglietta, M.M.,Rotunno, R., 2019. Development Mechanisms for Mediterranean Tropical-like  
697 Cyclones (Medicanes). *Q. J. R. Meteorol. Soc.* 145, 1444–1460.

698

699 Mishra, A.K.,Jangir, B. & Strobach, E.,2024. Influence of mesoscale sea-surface temperature structures  
700 on the Mediterranean cyclone Ianos in convection-permitting simulations: Contributions of surface  
701 warming and cold wakes. *Quarterly Journal of the Royal Meteorological Society*, 150(765), 5146–  
702 5166. <https://doi.org/10.1002/qj.4862>

703

704 Morrow, R., *et al.*,2019. "Global observations of fine-scale ocean surface topography with the Surface  
705 Water and Ocean Topography (SWOT) mission." *Frontiers in Marine Science*, 6, 232.  
706 <https://doi.org/10.3389/fmars.2019.00232>.

707

708 Nicolaides, K. A., Michalelides, S. C., and Karacostas, T. (2006). Synoptic and dynamic characteristics  
709 of selected deep depressions over Cyprus, *Adv. Geosci.*, 7, 175–180, <https://doi.org/10.5194/adgeo-7-175-2006>, 2006.

711

712 Normand, J.C.L., Heggy, E., 2024. Assessing flash flood erosion following storm Daniel in Libya. *Nat  
713 Commun* 15, 6493. <https://doi.org/10.1038/s41467-024-49699-8>

714

715 Oliver, E.C.J., Donat, M.G., Burrows, M.T. *et al.*, 2018. Longer and more frequent marine heatwaves  
716 over the past century. *Nat Commun* 9, 1324. <https://doi.org/10.1038/s41467-018-03732-9>

717

718 Panegrossi, G., D'Adderio, L. P., Dafis, S., Rysman, J.-F., Casella, D., Dietrich, S., & Sanò, P., 2023.  
719 Warm Core and Deep Convection in Medicanes: A Passive Microwave-Based Investigation. *Remote  
720 Sensing*, 15(11), 2838. <https://doi.org/10.3390/rs15112838>

721

722 Pytharoulis, I., Kartsios, S., Tegoulias, I., Feidas, H., Miglietta, M. M., Matsangouras, I., & Karacostas,  
723 T.,2018. Sensitivity of a Mediterranean Tropical-Like Cyclone to Physical Parameterizations.  
724 *Atmosphere*, 9(11), 436. <https://doi.org/10.3390/atmos9110436>

725

726 Raveh-Rubin, S. and Flaounas, E.,2017. A dynamical link between deep Atlantic extratropical cyclones  
727 and intense Mediterranean cyclones. *Atmospheric Science Letters*, 18: 215-221.  
728 <https://doi.org/10.1002/asl.745>

729

730 Reale, M., Cabos, W., Cavicchia, L., Conte, D., Coppola, E., Flaounas, E., *et al.*,2022. Future  
731 projections of Mediterranean cyclone characteristics using the Med-CORDEX ensemble of coupled



732 regional climate system models. *Climate Dynamics*, 58(9–10), 2501–2524.  
733 <https://doi.org/10.1007/s00382-021-06018-x>

734

735 Reynolds, R. W., Smith, T. M., Liu, C., Chelton, D. B., Casey, K. S., and Schlax, M. G., 2007. Daily  
736 High-Resolution-Blended Analyses for Sea Surface Temperature. *J. Climate*, 20, 5473–5496,  
737 <https://doi.org/10.1175/2007JCLI1824.1>.

738

739 Scardino, G., Kushabaha, A., Miglietta, M. M., Bonaldo, D., and Scicchitano, G.: When storms stir the  
740 Mediterranean depths: chlorophyll *a* response to Mediterranean cyclones, *Ocean Sci.*, 21, 2849–2872,  
741 <https://doi.org/10.5194/os-21-2849-2025>, 2025.

742

743 Scardino, G., Miglietta, M.M., Kushabaha, A. *et al.*,2024. Fingerprinting Mediterranean hurricanes  
744 using pre-event thermal drops in seawater temperature. *Sci Rep* 14, 8014.  
745 <https://doi.org/10.1038/s41598-024-58335-w>

746

747 Shang, X.-D., Zhu, H.-B., Chen, G.-Y., Xu, C., & Yang, Q.,2015. Research on cold core eddy change  
748 and phytoplankton bloom induced by typhoons: Case studies in the South China Sea. *Advances in  
749 Meteorology*, 1–19.doi: [10.1155/2015/340432](https://doi.org/10.1155/2015/340432).

750

751 Shang, X.-D., Zhu, H.-B., Chen, G.-Y., Xu, C., & Yang, Q.,2015. Research on cold core eddy change  
752 and phytoplankton bloom induced by typhoons: Case studies in the South China Sea. *Advances in  
753 Meteorology*, 1–19.doi: [10.1155/2015/340432](https://doi.org/10.1155/2015/340432).

754

755 Sharma, V., & Ali, M. M.,2014. Importance of ocean heat content for cyclone studies. *Journal of  
756 Climatology & Weather Forecasting*, 2(1), 1–6. [https://www.longdom.org/open-access/importance-of-  
ocean-heat-content-for-cyclone-studies-9577.html](https://www.longdom.org/open-access/importance-of-<br/>757_ocean-heat-content-for-cyclone-studies-9577.html)

758

759 Strobach, E., Mishra, A.K., Jangir, B. *et al.*, 2024. Intensification of a rain system imparted by  
760 Mediterranean mesoscale eddies. *Sci Rep* 14, 26810. <https://doi.org/10.1038/s41598-024-76767-2>

761

762 Stern, M., 1965, Interaction of a uniform wind stress with a geostrophic vortex, *Deep Sea Res. Oceanogr.  
763 Abstr.*, 12(3), 355–367.

764

765 Sun, M., Tian, F., Liu, Y., & Chen, G., 2017. An Improved Automatic Algorithm for Global Eddy  
766 Tracking Using Satellite Altimeter Data. *Remote Sensing*, 9(3), 206. <https://doi.org/10.3390/rs9030206>

767

768 Trigo, I. F., Bigg, G. R., and Davies, T. D., 2002. Climatology of cyclogenesis mechanisms in the  
769 Mediterranean, *Mon. Weather Rev.*, 130, 549–569.

770

771 Vidya, P. J., Balaji, M., Mani Murali, R., 2021. Cyclone Hudhud-eddy induced phytoplankton bloom  
772 in the northern Bay of Bengal using a coupled model, *Progress in Oceanography*, Volume 197, 102631,  
773 ISSN 0079-6611, <https://doi.org/10.1016/j.pocean.2021.102631>.

774

775 Volpe, G., Buongiorno Nardelli, B., Colella, S., Pisano, A. and Santoleri, R.,2018. An Operational  
776 Interpolated Ocean Colour Product in the Mediterranean Sea, in *New Frontiers in Operational  
777 Oceanography*, edited by E. P. Chassignet, A. Pascual, J. Tintorè, and J. Verron, pp. 227–244.

778



779 Volpe, G., Colella, S., Brando, V. E., Forneris, V., Padula, F. L., Cicco, A. D., & Santoleri, R., 2019.  
780 Mediterranean Ocean Colour Level 3 operational multi-sensor processing. *Ocean Science*, 15(1), 127-  
781 146.

782

783 Wada, A., & Usui, N., 2007. Impact of tropical cyclone heat potential on tropical cyclone intensity in  
784 the western North Pacific Ocean. *Journal of Oceanography*, 63(3), 505-516.  
785 <https://doi.org/10.1007/s10872-007-0039-0>

786

787 Wada, A., Usui, N., 2007. Importance of tropical cyclone heat potential for tropical cyclone intensity  
788 and intensification in the Western North Pacific. *J Oceanogr* 63, 427-447.  
789 <https://doi.org/10.1007/s10872-007-0039-0>

790

791 Tranchant, Y. T., Legresy, B., Foppert, A., et al., 2025. SWOT reveals fine-scale balanced motions and  
792 dispersion properties in the Antarctic Circumpolar Current. *ESS Open Archive* .  
793 [10.22541/essoar.173655552.25945463/v1](https://doi.org/10.22541/essoar.173655552.25945463/v1)

794

795 Zhang, Z., & Qiu, B., 2020. Surface Chlorophyll Enhancement in Mesoscale Eddies by Submesoscale  
796 Spiral Bands. *Geophysical Research Letters*, 47, e2020GL088820.  
797 <https://doi.org/10.1029/2020GL088820>

798

799 Zhao et al., 2019. A MATLAB toolbox to detect and analyze marine heatwaves. *Journal of Open Source  
800 Software*, 4(33), 1124, <https://doi.org/10.21105/joss.01124>

801

802 Zittis, G., Almazroui, M., Alpert, P., Ciais, P., Cramer, W., Dahdal, Y., et al., 2022. Climate change and  
803 weather extremes in the Eastern Mediterranean and Middle East. *Reviews of Geophysics*, 60(3),  
804 e2021RG000762. <https://doi.org/10.1029/2021RG000762>.

805

806

807